Journal of Science and Transport Technology
Journal homepage: https://jstt.vn/index.php/en

UNIVERSITY OF TRANSPORT TECHNOLOGY

Thermomechanical vibration of sandwich beams with FGP core based on a Timoshenko beam formulation

Nguyen Dinh Kien[1,3], Le Thi Ngoc Anh[2*]
[1]VNU University of Engineering and Technology, 144 Xuan Thuy, Hanoi, Vietnam
[2]HUTECH Institute of Engineering, HUTECH University, 475A Dien Bien Phu, Thanh My Tay Ward, Ho Chi Minh City, Vietnam
[3]Institute of Mechanics, VAST, 18 Hoang Quoc Viet, Hanoi, Vietnam

Article info
Type of article:
Original research paper

DOI:
https://doi.org/10.58845/jstt.utt.2026.en.6.4.36-50

[*]**Corresponding author:**
Email address:
ltn.anh90@hutech.edu.vn

Received: 06/12/2025
Received in Revised Form: 01/06/2026
Accepted: 22/06/2026

Abstract: This paper investigates the thermomechanical vibration of sandwich beams with isotropic homogeneous face layers and a core of porous material by using a Timoshenko finite element beam formulation. The material properties of the sandwich beams are dependent on the environmental temperature, and the porosity distribution in the core through the beam thickness follows a cosine function. Applying the finite element method, a beam element formulation is derived and used to construct the discretized motion equation. The present formulation employs the solution of the homogeneous equilibrium equations to approximate the rotation and deflection of the beams, which helps to improve the efficiency and to avoid the shear-locking problem. The finding emphasizes the significant impact of the environmental temperature and the porous parameter on the thermomechanical vibration responses. A detailed investigation is presented to illustrate the effects of the temperature variations, the porous coefficient, the specific beam configuration, and the ratio of span to height of the beam on the vibration of the sandwich beams.

Keywords: Porous material, Timoshenko beam, thermoelastic vibration.

1. Introduction

With the development of advanced manufacturing methods, a new lightweight material, namely functionally graded porous (FGP) material, has been introduced to improve the performance of structures. Different from natural porous materials, porosities in this material are intentionally introduced into the material for improve its properties. As a result, the density of the FGP material is low, while the physical and mechanical properties are significantly improved. FGP material has a high capacity for energy absorption, and it is widely used in the manufacture of sandwiches to reduce vibration or enhance the impact resistance of structural elements. Many advanced properties and applications of FGP material can be found in Refs. [1, 2].

A porous structure can be designed such that the porosities smoothly and gradually vary in one or more desired directions. The mechanical properties of the resulting FGP structure change according to porosity parameters, and they can be tailored to optimize the performance of the structure. Compared to conventional structures, an FGP structure possesses many advantageous characteristics, such as lightweight, heat and sound insulation, vibration improvement… The mechanical responses of functionally graded porous FGP structures have attracted significant research interest in recent years. A brief discussion of papers most relevant to this study follows.

Ref. [3] applied the Chebyshev method in studying the vibration of FGP beam structure. The effects of non-classical boundary conditions, namely the elastic end conditions and the various patterns of distribution of porosities in the vibration response, have been considered by the authors. In Refs. [4, 5], Chen and his co-workers employed the Ritz approach to establish the fundamental equations for exploring the behavior of FGP beams in bending, buckling, and vibration. The authors employed Timoshenko beam theory to describe beam deformation and investigated in detail the effects of porosity parameters on the beam responses. Srikarun et al. [6] employed the third-order shear deformable theory of Reddy to develop a beam model to investigate the linear and nonlinear behavior of sandwich beams with an FGP core in bending, demonstrating the important role of porosity distribution, loading type, and aspect ratio on the behavior of the sandwich beams. In Ref. [7], Chen and his co-workers explored the nonlinear behavior in vibration response of sandwich porous beams, using the Ritz method to construct the nonlinear discretized equation of motion.

It has been revealed that changes in temperature have an impact on the mechanical responses of structures. Regarding beam structure, the structure considered in the present work, Chen and his co-workers [8] investigated the thermomechanical vibration of high-order FG beams, showing the significant influence of temperature on the vibration response of the beams. Trinh et al. [9] applied the state space approach in their study of buckling and vibration of graded beams subjected to mechanical and thermal loading, revealing the negative effect of temperature on the frequencies and buckling loads. Wattanasakulpong et al. [10] also investigated the buckling and vibrational problems of the FG beams, applying the Ritz method in solving the eigenvalue problems for the critical loads and natural frequencies. Their numerical investigation reveals that the beam frequency declines when the temperature increases, and it approaches zero when the temperature increases toward the critical load. Zhang [11] took into consideration the exact physical position of the neutral surface in deriving the governing equations in their thermal post-buckling and nonlinear vibration analysis of FG beams, showing a declining tendency of both the post-critical strength and the ratio between the nonlinear frequencies and the linear frequencies. Eiadtrong and co-workers [12] applied the modified Fourier method in their thermomechanical vibration study of FGP beams with elastic end constraints. Their investigations reveal the important role of the porous parameter, pattern of porosity distribution, and temperature on the vibration responses.

One can see from the above review of literature that the changes in temperature have an impact on the vibration responses of the beam structure. Different from the graded beams discussed above, the sandwich beams considered herein contain porosities, which are intentionally introduced into the beams to improve their performance, especially the vibration responses in a thermal environment. Motivated by the fact that the simultaneous influence of temperature and porosity variations on the vibration of functionally graded porous beams has not been explored, this paper investigates the thermo-elastic vibration of sandwich beams featuring a core made from an FGP material. The present study assumes that the material properties of the considered sandwich beams are sensitive to the temperature of the environment, and the porosities are distributed by a cosine function through the beam thickness. The motion equation for the study is derived in terms of the finite element analysis in the framework of Timoshenko's beam theory. Natural frequencies are obtained for the beam with different ratios of length-to-thickness, and the effects of the porosity parameter, the temperature change, and the beam configuration on the vibration behavior of the FGP sandwich beam are investigated and discussed.

2. Mathematical model

2.1. Sandwich beams in thermal environment

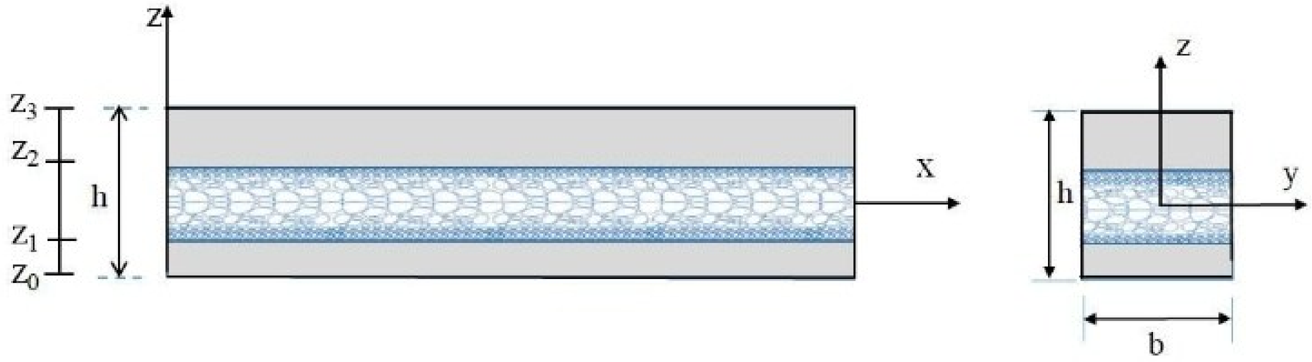

Fig. 1. A sketch of sandwich beam featuring an FGP core layer

Fig. 1 shows a sandwich beam consisting of two isotropic face layers and a core made from an FGP material. The geometry of the beam is defined by a rectangular cross-section, characterized by width b and total thickness h. As shown in Fig. 1, the coordinate system (x,y,z) is established with the (x,y) plane aligned wuth the mid-plane of the beam. The notations z_0, z_1, z_2 and z_3, where $z_0 = -h/2$ and $z_3 = h/2$, in Fig. 1 respectively denote the coordinates from the (x,y) plane of the bottommost surface, the interface surfaces between the layers, and the topmost surface.

The present study considers that the sandwich beam is placed in a thermal environment with a temperature T. The beam material properties are sensitive to the environmental temperature, and an intrinsic property (Π), specifically the elastic modulus E, the density of mass ρ, the Poisson's ratio (ν), and the thermal expansion coefficient (α), varies with temperature as follows [13].

$$\Pi = \Pi_0\left(\Pi_{-1}T^{-1} + 1 + \Pi_1 T^1 + \Pi_2 T^2 + \Pi_3 T^3\right) \qquad (1)$$

where $\Pi_0, \Pi_{-1}, \Pi_1, \Pi_2,$ and Π_3 are material coefficients which are dependent on the temperature; $T = T_0 + \Delta T$, with T_0 (taken by 300K) is the reference temperature, and ΔT is the rise in temperature.

In this study, we assume that the effective properties, including the effective elastic Young's modulus, shear modulus, and the effective mass density of the sandwich beam, obey the following rule

$$\begin{cases} E_f(T) = E_1(T) \\ G_f(T) = G_1(T) \quad \text{for } z \in [z_0, z_1] \text{ and } z \in [z_2, z_3] \\ \rho_f(T) = \rho_1(T) \end{cases}$$

$$\begin{cases} E_f(z,T) = E_1(T)\left[1 - e_0 \cos\left(\dfrac{\pi z}{z_2 - z_1}\right)\right] \\ G_f(z,T) = G_1(T)\left[1 - e_0 \cos\left(\dfrac{\pi z}{z_2 - z_1}\right)\right] \quad \text{for } z \in [z_1, z_2] \\ \rho_f(z,T) = \rho_1(T)\left[1 - e_m \cos\left(\dfrac{\pi z}{z_2 - z_1}\right)\right] \end{cases} \qquad (2a)$$

$$\begin{cases} E_f(T) = E_1(T) \\ G_f(T) = G_1(T) \quad \text{for } z \in [z_0, z_1] \text{ and } z \in [z_2, z_3] \\ \rho_f(T) = \rho_1(T) \end{cases}$$

$$\begin{cases} E_f(z,T) = E_1(T)\left[1 - e_0 \cos\left(\dfrac{\pi z}{2(z_2 - z_1)} + \dfrac{\pi}{4}\right)\right] \\ G_f(z,T) = G_1(T)\left[1 - e_0 \cos\left(\dfrac{\pi z}{2(z_2 - z_1)} + \dfrac{\pi}{4}\right)\right] \quad \text{for } z \in [z_1, z_2] \\ \rho_f(z,T) = \rho_1(T)\left[1 - e_m \cos\left(\dfrac{\pi z}{2(z_2 - z_1)} + \dfrac{\pi}{4}\right)\right] \end{cases} \qquad (2b)$$

In the preceding equations E_1 and ρ_1 represent the maximum Young's modulus and mass density, respectively. The corresponding maximum shear modulus is derived as $G_1 = E_1 / 2(1+\nu)$, where ν denotes the Poisson's ratio. Furthermore, e_0 and e_m signify the coefficients of porosity and mass, which are determined by the following formulas [5]

$$e_0 = 1 - \frac{E_0}{E_1},\ e_m = 1 - \frac{\rho_0}{\rho_1} \quad (0 < e_0 < 1,\ 0 < e_m < 1) \tag{3}$$

In these expressions, E_0 and ρ_0 represent the minimum values of Young's modulus and the mass density, respectively. For an open-cell metal foam, the relationship between these two properties is defined as follows [5]

$$\frac{E_0}{E_1} = \left(\frac{\rho_0}{\rho_1}\right)^2 \tag{4}$$

From Eqs. (3) and (4), one can obtain the relationship between the coefficient of Young's modulus e_0 and that of the mass density e_m in the form

$$e_m = 1 - \sqrt{1 - e_0} \tag{5}$$

Of course, the coefficient for Young's modulus, as mentioned in Eq. (3), satisfies the condition $e_0<1$.

2.2. Governing equations

According to Timoshenko beam theory, the displacement components (u_x and u_z) at any point within the beam along the x and z axes are of the following form

$$\begin{cases} u_x = u_{x0}(x,t) - z\theta(x,t) \\ u_z = u_{z0}(x,t) \end{cases} \tag{6}$$

In this expresion, u_{x0} and u_{z0} represent the mid-plane displacements in the x and z directions, respectively, while $\theta(x,t)$ denotes the rotation of the beam cross section.

Eq. (6) gives the normal strain (ε_{xx}) and the shear strain (γ_{xz}) of the form

$$\varepsilon_{xx} = u_{x0,x} - z\theta_{,x},\quad \gamma_{xz} = u_{z0,x} - \theta \tag{7}$$

In the above equation and in the below, the comma subscript notation is used to denote partial differentiation with respect to the subsequent variable, for instance $u_{x0,x} = \partial u_{x0} / \partial x$. Based on the linear elastic behavior of the beam material, the normal and shear stresses related to the strains in Eq. (7) are defined as follows

$$\sigma_{xx} = E_f \varepsilon_{xx},\qquad \tau_{xz} = \psi G_f \gamma_{xz} \tag{8}$$

where and τ_{xz} are, respectiveky, the normal and shear stresses; ψ denotes the factor of shear correction, which is needed to introduce for compensating the constant shear stress in the beam thickness in the Timoshenko beam theory. The value of the coefficient ψ is chosen depending on the geometry of the beam cross section, and it is selected by 5/6 for the rectangular section beam of the present work.

From Eqs. (7) and (8), one can write the elastic strain energy of the beam in the following form

$$U_B = \int_0^L \int_A (\sigma_{xx}\varepsilon_{xx} + \tau_{xz}\gamma_{xz})\, dS dx$$
$$= \int_0^L \left[D_{11} u_{x0,x}^2 - 2D_{12} u_{x0,x}\theta_{,x} + D_{22}\theta_{,x}^2 + \psi D_{33}\left(u_{z0,x} - \theta\right)^2 \right] dx \tag{9}$$

with A is the cross-sectional area; D_{11}, D_{12}, D_{22} and D_{33} are the stretching, stretching-bending coupling, bending, and shear rigidities of the beam, and they are defined as follows

$$\left(D_{11}, D_{12}, D_{22}\right) = \sum_{k=1}^{3} \int_{z_{k-1}}^{z_k} bE_f\left(1,\ z,\ z^2\right) dz;$$
$$D_{33} = \sum_{k=1}^{3} \int_{z_{k-1}}^{z_k} bG_f dz \tag{10}$$

The elastic energy resulting from the temperature change can be written in the form

$$U^T = \frac{1}{2}\int_0^L N^T u_{z0,x}^2 dx \tag{11}$$

where N^T denotes the thermal resultant, which is calculated as follows

$$N^T = -\sum_{k=1}^{3} \int_{z_{k-1}}^{z_k} bE_f \alpha \Delta T dz \tag{12}$$

The beam's to kinetic energy, denoted by (K), is defined as follows

$$K = \frac{1}{2}\int_0^L \int_A \rho_f \left(\dot{u}_x^2 + \dot{u}_z^2\right) dSdx = \frac{1}{2}\int_0^L \left[J_{11}\left(\dot{u}_{x0}^2 + \dot{u}_{z0}^2\right) - 2J_{12}\dot{u}_{x0}\dot{\theta} + J_{22}\dot{\theta}^2 \right] dx \tag{13}$$

where J_{11}, J_{12}, J_{22} are the mass moments, and they are defined as follows

$$\left(J_{11}, J_{12}, J_{22}\right) = \sum_{k=1}^{3} \int_{z_{k-1}}^{z_k} b\rho_f \left(1, z, z^2\right) dz \tag{14}$$

With the energy expressions in Eqs. (9), (11) and (13), one can obtain the differential motion equations by using Hamilton's principle, and they have the following form

$$\begin{cases} J_{11}\ddot{u}_{x0} - J_{12}\ddot{\theta} - D_{11}u_{x0,x} + D_{12}\theta_{,xx} = 0 \\ J_{11}\ddot{u}_{z0} - \psi D_{33}\left(u_{zo,xx} - \theta_{,x}\right) - N^T u_{z0.xx} = 0 \\ J_{22}\ddot{\theta} - J_{12}\ddot{u}_{x0} + D_{12}u_{x0,xx} - D_{22}\theta_{,xx} - \psi D_{33}\left(u_{z0,x} - \theta\right) = 0 \end{cases} \tag{15}$$

The derivation of an analytical solution for equation (15) is cumbersome. The present paper applies the finite element method for solving Eq. (15).

3. Solution method

This section derives a finite element beam model for solving the system of equations (15). To this end, we consider herewith a two-node beam element with length of l. The vector of nodal degree of freedom for the element is of the form

$$\underset{(6\times1)}{\mathbf{d}_e} = \left\{\mathbf{d}_a \ \mathbf{d}_b\right\}^T \tag{16}$$

with $\mathbf{d}_a = \left\{u_{x01} \ u_{x02}\right\}^T$; $\mathbf{d}_b = \left\{u_{z01} \ \theta_1 \ u_{z02} \ \theta_2\right\}^T$

where $\mathbf{d}_a$ denotes the vector of axial displacements at the nodes; and $\mathbf{d}_b$ is the vector of bending displacements and rotation at the nodes; u_{x0i}, u_{z0i}, and θ_i (i=1,2) are, respectively, the displacements in the x and z directions, and the rotations at the node i.

Following the standard method of the finite element method, we introduce the interpolations for the displacements and rotation as follows

$$u_{x0} = \mathbf{H}_a\mathbf{d}_a, \ u_{z0} = \mathbf{H}_b\mathbf{d}_b, \ \theta = \mathbf{H}_\theta\mathbf{d}_b \tag{17}$$

where $\mathbf{H}_a = \left\{H_{a1} H_{a2}\right\}$, $\mathbf{H}_b = \left\{H_{b1} H_{b2} H_{b3} H_{b4}\right\}$, and $\mathbf{H}_\theta = \left\{H_{\theta_1} H_{\theta2} H_{\theta_3} H_{\theta4}\right\}$ respectively denote the matrices of interpolating functions for the displacement u_{x0}, u_{z0}, and the rotation θ, respectively. Conventionally, linear functions can be used for both the displacements and the rotation since these quantities are independent in the Timoshenko beam theory. The beam formulation built from the linear interpolation, however, suffers from the shear-locking problem and poor convergence [14]. In order to avoid the shear-locking problem and to improve the efficiency of the formulation, the quadratic and cubic polynomials, obtained by solving the equilibrium equations of a beam element, are adopted in the present paper for the rotation and transverse displacement, while linear functions are still used for the axial displacement. The detail derivation of the interpolating functions for the rotation and transverse displacement can be found in Ref. [15]. The expressions for the interpolating functions are as follows [15].

- Interpolating functions for the axial displacement u_{x0}:

$$H_{a1} = \frac{x}{l}, \ H_{a2} = \frac{1-x}{l}. \tag{18}$$

- Interpolating functions for the bending displacement u_{z0}:

$$\begin{aligned} H_{b1} &= \frac{1}{(1+\lambda)}\left[2\left(\frac{x}{l}\right)^3 - 3\left(\frac{x}{l}\right)^2 - \lambda\left(\frac{x}{l}\right) + (1+\lambda)\right], \\ H_{b2} &= \frac{l}{(1+\lambda)}\left[\left(\frac{x}{l}\right)^3 - \left(2+\frac{\lambda}{2}\right)\left(\frac{x}{l}\right)^2 - \left(2+\frac{\lambda}{2}\right)\left(\frac{x}{l}\right)\right], \\ H_{b3} &= \frac{1}{(1+\lambda)}\left[\left(\frac{x}{l}\right)^3 - 3\left(\frac{x}{l}\right)^2 - \lambda\left(\frac{x}{l}\right)\right], \\ H_{b4} &= \frac{l}{(1+\lambda)}\left[\left(\frac{x}{l}\right)^3 - \left(1-\frac{\lambda}{2}\right)\left(\frac{x}{l}\right)^2 - \frac{\lambda}{2}\left(\frac{x}{l}\right)\right]. \end{aligned} \tag{19}$$

- Interpolating functions for the rotation θ

$$H_{\theta_1} = \frac{6}{(1+\lambda)l}\left[\left(\frac{x}{l}\right)^2 - \left(\frac{x}{l}\right)\right],$$
$$H_{\theta_2} = \frac{1}{(1+\lambda)}\left[3\left(\frac{x}{l}\right)^2 - (4+\lambda)\left(\frac{x}{l}\right) + (1+\lambda)\right],$$
$$H_{\theta_3} = \frac{6}{(1+\lambda)l}\left[\left(\frac{x}{l}\right)^2 - \left(\frac{x}{l}\right)\right],$$
$$H_{\theta_4} = \frac{1}{(1+\lambda)}\left[3\left(\frac{x}{l}\right)^2 - (2+\lambda)\left(\frac{x}{l}\right)\right]. \tag{20}$$

In Eqs. (19) and (20), $\lambda = 12D_{22}/\left(l^2\psi D_{33}\right)$ is the shear deformation parameter.

In substituting the above interpolating functions into the expression of elastic energy in Eq. (9), one can obtain a matrix form for the energy as follows

$$U = \frac{1}{2}\sum^{nE}\mathbf{d}_e^T\mathbf{k}_e\mathbf{d}_e, \tag{21}$$

where nE is the number of beam elements used to discretize the beam; $\mathbf{k}_e$ is the element matrix of stiffness, and it can be split into submatrices as follows

$$\mathbf{k}_e = \begin{bmatrix} \mathbf{k}_{e_{aa}} & \mathbf{k}_{e_{ab}} \\ \mathbf{k}_{e_{ab}}^T & \mathbf{k}_{e_{bb}} + \mathbf{k}_{e_{ss}} \end{bmatrix}, \tag{22}$$

in which $\mathbf{k}_{e_{aa}}$, $\mathbf{k}_{e_{ab}}$, $\mathbf{k}_{e_{bb}}$ and $\mathbf{k}_{e_{ss}}$ are, respectively, the element matrices of stiffness, which result from the axial stretching, coupling between the axial stretching and bending, bending, and shear deformation. The expressions of these submatrices are as follows

$$\mathbf{k}_{e_{aa}} = \int_0^l H_{a,x}^T D_{11} H_{a,x} dx,\ \mathbf{k}_{e_{ab}} = -\int_0^l H_{a,x}^T D_{12} H_{\theta,x} dx,$$
$$\mathbf{k}_{e_{bb}} = \int_0^l H_{\theta,x}^T D_{22} H_{\theta,x} dx, \tag{23}$$
$$\mathbf{k}_{e_{ss}} = \int_0^l \left(H_{b,x} - H_\theta\right)^T \psi D_{33} \left(H_{b,x} - H_\theta\right) dx$$

In substituting the interpolating functions into the expression of kinetic energy in Eq. (13), one can obtain a matrix form for the kinetic energy as follows

$$K = \frac{1}{2}\sum^{nE}\dot{\mathbf{d}}_e^T\mathbf{m}_e\dot{\mathbf{d}}_e, \tag{24}$$

where the mass matrix of the element $\mathbf{m}$ can be split in submatrices as follows:

$$\mathbf{m}_e = \begin{bmatrix} \mathbf{m}_{e_{aa}} & \mathbf{m}_{e_{a\theta}} \\ \mathbf{m}_{e_{a\theta}}^T & \mathbf{m}_{e_{\theta\theta}} + \mathbf{m}_{e_{bb}} \end{bmatrix}, \tag{25}$$

with

$$\mathbf{m}_{e_{aa}} = \int_0^l H_a^T J_{11} H_a dx,\ \mathbf{m}_{e_{bb}} = \int_0^l H_b^T J_{11} H_b dx,$$
$$\mathbf{m}_{e_{a\theta}} = -\int_0^l H_a^T J_{12} H_\theta dx,\ \mathbf{m}_{e_{\theta\theta}} = \int_0^l H_\theta^T J_{22} H_\theta dx \tag{26}$$

The mass submatrices in the above equation result from the translations in the x direction and z direction, the coupling between the translation in the x direction and the rotation of cross section, and the rotation of cross section, respectively.

The energy U^T due to the temperature change in Eq. (12) can also be written in a matrix form as

$$U^T = \frac{1}{2}\sum^{nE}\mathbf{d}_e^T\mathbf{k}_e^T\mathbf{d}_e, \tag{27}$$

where $\mathbf{k}_e^T$ is the element matrix of stiffness resulted from the change of temperature, and it has the following form

$$\mathbf{k}_e^T = \begin{bmatrix} 0 & 0 \\ 0 & \mathbf{k}_{e_{bb}}^T \end{bmatrix}, \tag{28}$$

with

$$\mathbf{k}_{e_{bb}}^T = \int_0^l \mathbf{H}_{b,x}^T N^T \mathbf{H}_{b,x} dx \tag{29}$$

With the above derived element matrices, one can construct the motion equations for the analysis of the sandwich beam in vibration, and it can be expressed in the form

$$\mathbf{M}_g\ddot{\mathbf{D}}_g + \left(\mathbf{K}_g + \mathbf{K}_g^T\right)\mathbf{D}_g = \mathbf{0} \tag{30}$$

In Eq. (30), $\mathbf{D}_g$ and $\ddot{\mathbf{D}}_g$ represent the global displacement and acceleration vectors at the nodes, respectively, while $\mathbf{M}_g$, $\mathbf{K}_g$, and $\mathbf{K}_g^T$ are, respectively, the global matrices of mass, stiffness, and thermal stiffness. By assuming a harmonic vibration for the displacement, Eq. (30) transforms into an eigenvalue problem, and solving it by by the standard method described in some well-known textbooks, e.g. Ref. [16] gives the natural frequencies.

4. Numerical Investigation

For numerical investigation, we adopted a sandwich beam made from steel with a rectangular section (bxh)=(1x1) m^2 and different aspect ratios. We employ three numbers in parentheses to denote the ratio of the layer thickness. For instance, the notation (2-1-2) means that the thickness ratio of the bottom layer, the core, and the top layer is $(h_1 : h_2 : h_3) = (2-1-2)$. The properties of the beam material which are temperature-dependent, are adopted from Ref. [17] and they are listed in Table 1. The sandwich beam with three different boundary conditions, namely simply supported (referred to as SS beam), clamped-clamped (referred to as CC beam), and clamped-supported (referred to as CS beam), is considered. The constraints for these bondary conditions are as follows:

$u_{x0}(0,t) = u_{z0}(0,t) = u_{z0}(L,t) = 0$ for SS beam

$u_{x0}(0,t) = u_{x0}(L,t) = 0,\ u_{z0}(0,t) = u_{z0}(L,t) = 0$ and $\theta(0,t) = \theta(L,t) = 0$ for CC beam

$u_{x0}(0,t) = u_{z0}(0,t) = u_{z0}(L,t) = 0$ and $\theta(0,t) = 0$ for CS beam

For the sake of discussion convenience, we introduce the dimensionless parameter for the frequencies as follows

$$\mu_i = \omega_i \frac{L^2}{h}\sqrt{\frac{\rho}{E}} \tag{31}$$

In the above equation ω_i denotes the i^{th} vibration frequency; ρ is the material density, and E is the elastic modulus of the beam material at the reference temperature, that is at 300 K.

4.1. Accuracy and Convergence Studies

The reliability of the current beam formulation is validated in this work through a comparison of the first frequency parameters of an FGP beam in a thermal environment predicted by the formulated formulation with the data reported in Ref. [12], and the results are shown in Table 2. As shown in Table 2, the natural frequencies calculated using the present formulation demonstrate excellent agreement with the results reported in Ref. [12]. This observation remains consistent across all three boundary conditions and throughout the entire range of temperature variations considered. It is noted that Ref. [12] employed the third-order shear deformable beam theory and the modified Fourier method in predicting the natural frequencies.

The convergent behavior of the derived beam formulation in prediction of the first frequency parameters of the SS, CC, and CS sandwich beams with an FGP core is shown in Tables 3-5 for a span-to-thickness ratio L/h =10, and a value of the temperature change ΔT = 30 K. As observed from these tables, the convergence of the derived beam formulation is quite fast, and the frequencies can be predicted by using twenty beam elements. This conclusion is correct for all three boundary conditions and all the considered porosity coefficients. With this convergence result, we will use twenty elements for discretizing the sandwich beam in all the computations reported below.

4.2. Numerical results

Table 1. The temperature-dependent coefficients of the beam material [17]

Properties	Π_0	Π_{-1}	Π_1	Π_2	Π_3
$E\,(Pa)$	201×10^9	0	3.08×10^{-4}	-6.53×10^{-7}	0
$\rho\ (kg/m^3)$	8166	0	0	0	0
$\alpha\left(K^{-1}\right)$	1.23×10^{-5}	0	8.09×10^{-4}	0	0
ν	0.3262	0	-2.02×10^{-4}	3.797×10^{-7}	0

Table 2. Verification of the formulated beam formulation in prediction of the first frequency parameter of FGP beam (L/h=10)

BCs	e_0	ΔT=0		ΔT=100		ΔT=200	
		Ref. [12]	Present	Ref. [12]	Present	Ref. [12]	Present
SS	0.2	0.2785	0.2786	0.2426	0.2428	0.2003	0.2005
	0.4	0.2784	0.2788	0.2452	0.2457	0.2066	0.2072
	0.6	0.2806	0.2815	0.2502	0.2513	0.2156	0.2168
	0.8	0.2884	0.2908	0.2609	0.2635	0.2301	0.2330
CC	0.2	0.5863	0.5961	0.5676	0.5771	0.5481	0.5574
	0.4	0.5806	0.5941	0.5633	0.5764	0.5452	0.5581
	0.6	0.5764	0.5965	0.5604	0.5803	0.5439	0.5635
	0.8	0.5758	0.6109	0.5612	0.5962	0.5461	0.5810

Table 3. Convergent performance of the current formulation in calculating the first frequency parameter of SS beam (L/h =10, ΔT =30 K)

Beam	e_0	nE=8	nE=10	nE=12	nE=14	nE=16	nE=18	nE=20	nE=22
(2-1-2)	0.2	2.7340	2.7338	2.7337	2.7337	2.7336	2.7336	2.7336	2.7336
	0.4	2.7556	2.7554	2.7553	2.7552	2.7552	2.7552	2.7551	2.7551
	0.8	2.8169	2.8166	2.8165	2.8164	2.8164	2.8163	2.8163	2.8163
(4-3-2)	0.2	2.7399	2.7397	2.7396	2.7395	2.7395	2.7394	2.7394	2.7394
	0.4	2.7668	2.7666	2.7665	2.7664	2.7664	2.7663	2.7663	2.7663
	0.8	2.8356	2.8353	2.8352	2.8351	2.8351	2.8350	2.8350	2.8350

Table 4. Convergent performance of the formulated formulation in calculating the first frequency parameter of CC beam (L/h =10, ΔT =30 K)

Beam	e_0	nE=8	nE=10	nE=12	nE=14	nE=16	nE=18	nE=20	nE=22
(2-1-2)	0.2	6.0309	6.0290	6.0280	6.0274	6.0270	6.0268	6.0266	6.0266
	0.4	6.0681	6.0660	6.0650	6.0643	6.0639	6.0636	6.0633	6.0633
	0.8	6.1808	6.1784	6.1771	6.1763	6.1758	6.1755	6.1752	6.1752
(4-3-2)	0.2	6.0429	6.0410	6.0399	6.0393	6.0390	6.0387	6.0385	6.0385
	0.4	6.0908	6.0887	6.0876	6.0870	6.0866	6.0863	6.0861	6.0861
	0.8	6.2180	6.2155	6.2141	6.2133	6.2128	6.2124	6.2121	6.2121

Table 5. Convergent performance of the formulated formulation in calculating the first frequency parameter of CS beam (L/h =10, ΔT =30 K)

Beam	e_0	nE=8	nE=10	nE=12	nE=14	nE=16	nE=18	nE=20	nE=22
(2-1-2)	0.2	4.2397	4.2390	4.2386	4.2384	4.2383	4.2382	4.2381	4.2381
	0.4	4.2691	4.2684	4.2680	4.2678	4.2676	4.2675	4.2675	4.2675
	0.8	4.3556	4.3547	4.3542	4.3539	4.3537	4.3536	4.3535	4.3535
(4-3-2)	0.2	4.2483	4.2476	4.2473	4.2471	4.2469	4.2468	4.2468	4.2468
	0.4	4.2857	4.2849	4.2845	4.2843	4.2841	4.2840	4.2840	4.2840
	0.8	4.3827	4.3818	4.3813	4.3810	4.3808	4.3807	4.3806	4.3806

Table 6. The fundamental frequency parameters of SS beam with various sandwich configurations for different e_0 and ΔT

		L/h =5		L/h =20	
e_0	ΔT	(1-2-1)	(4-3-1)	(1-2-1)	(4-3-1)
0.2	0	2.7013	2.7060	2.8722	2.8728
	50	2.6595	2.6632	2.2821	2.2616
	100	2.6110	2.6135	1.4163	1.3462
0.4	0	2.7343	2.7358	2.9165	2.9079
	50	2.6938	2.6932	2.3562	2.3058
	100	2.6467	2.6439	1.5623	1.4186
0.6	0	2.7793	2.7647	2.9756	2.9424
	50	2.7402	2.7225	2.4438	2.3489
	100	2.6944	2.6734	1.7134	1.4871
0.8	0	2.8499	2.7929	3.0647	2.9762
	50	2.8117	2.7509	2.5582	2.3910
	100	2.7669	2.7021	1.8818	1.5522

Table 7. The fundamental frequency parameters of CC beam with various sandwich configurations for different e_0 and ΔT

		L/h =5		L/h =20	
e_0	ΔT	(1-2-1)	(4-3-1)	(1-2-1)	(4-3-1)
0.2	0	5.1969	5.2257	6.4222	6.4252
	50	5.1619	5.1901	6.1085	6.1018
	100	5.1171	5.1445	5.7501	5.7319
0.4	0	5.2199	5.2657	6.5158	6.4989
	50	5.1856	5.2301	6.2154	6.1789
	100	5.1414	5.1846	5.8728	5.8134
0.6	0	5.2604	5.3034	6.6415	6.5693
	50	5.2267	5.2679	6.3538	6.2526
	100	5.1830	5.2223	6.0263	5.8911
0.8	0	5.3421	5.3388	6.8330	6.6365
	50	5.3087	5.3034	6.5563	6.3229
	100	5.2652	5.2578	6.2418	5.9652

In Tables 6-8, the parameters for the first frequencies of the sandwich porous beam with different sandwich configurations are presented for two span-to-height ratios, namely L/h = 5 and L/h = 20, and various values of the porosity parameter e_0 and the temperature change ΔT. Based on the tabulated results, several observations can be drawn regarding the influence of the sandwich configuration, porosity distribution, and temperature increments on the frequency parameters. Firstly, the parameter of the first frequencies remarkably intensifies when enlarging the porosity parameter e_0, irrespective of the boundary conditions and the temperature change. The enlargement of the porosity coefficient e_0 results in a decline in both the beam stiffness and weight, but the reduction of the weight is more significant than that of the stiffness, and this explains the enhancement of the frequency parameter by enlarging the parameter e_0. For all three types of boundary conditions considered herein and for a given value of the porosity parameter e_0, the enlargement of temperature yields a sharp reduction of the first frequency parameter. This tendency is expected since the increase in temperature leads to a decrease in the elastic moduli of the material, while the mass density is unchanged. As a result, the beam stiffness declines when the beam is subjected to a higher temperature, but the mass moments are unchanged. This explains the decrease in the frequency of the beam when it is placed in a higher temperature environment. The effects of the sandwich configuration and the boundary conditions are also clearly seen from Tables 6-8. The sandwich configuration can change the frequency parameter significantly, but the effect of the sandwich configuration is governed by the beam aspect ratio and the temperature rise. The frequency parameter of the (1-2-1) beam with L/h=5 is always higher than the corresponding value of the (4-3-1) beam, but the situation is opposite for the beam with L/h=20. The effect of the end constraints on the vibration response is expected, and the frequency parameters of the CC beam are the highest, while those of the SS beam are the lowest.

The impact of the porosity parameter on the thermomechanical vibration of the (1-2-1) sandwich beam can be observed from Figs. 2-4, where the first three frequency parameters of the sandwich beam are presented for the beam having a ratio of span-to-height of L/h =10 and different values of the temperature change. Examining the figures in more carefully reveals that all the first three parameters of frequencies of the sandwich beam increase by enlarging the coefficient of porosities, regardless of the temperature rise. The figures also demonstrate the sharp impact of the environmental temperature and porosity on the free vibration of the sandwich beam, and the difference between the frequencies caused by the temperature change tends to be lessened when enlarging the porous coefficient, and this tendency becomes more remarkable for the higher-order frequencies. In other words, the frequency of the beam with a larger porosity coefficient is less sensitive to the change of temperature, and this can be explained by the non-conductive air inside the porosities. It is emphasized that all the above remarks are correct for all three boundary conditions considered herein.

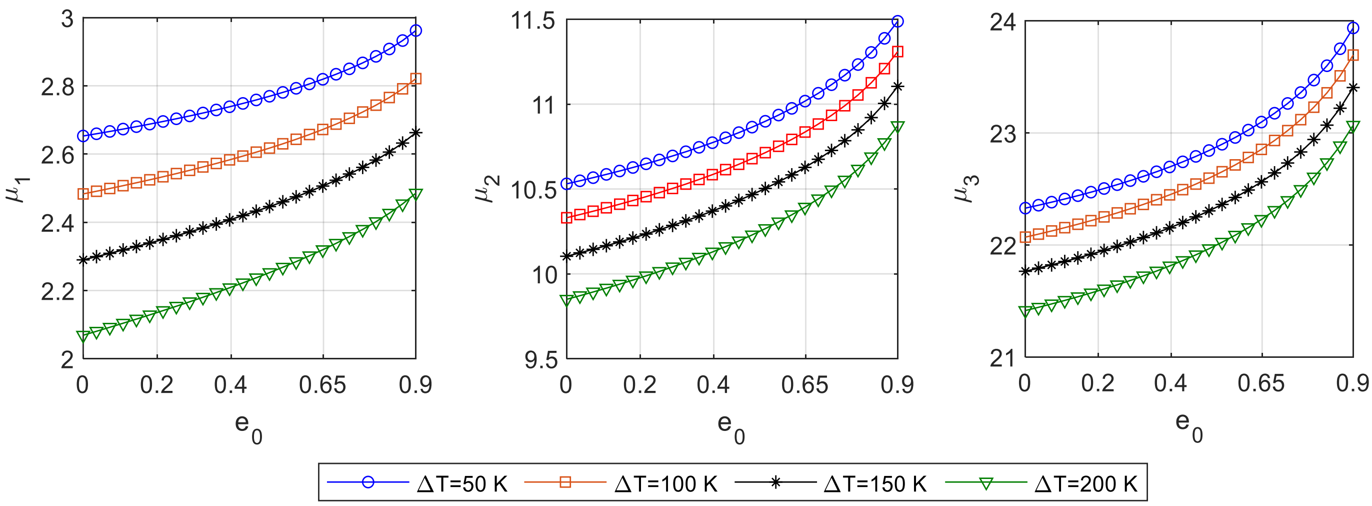

Fig. 2. The first three frequency parameters of SS (1-2-1) porous beam with porosity coefficients for L/h =10 and various values of the temperature change

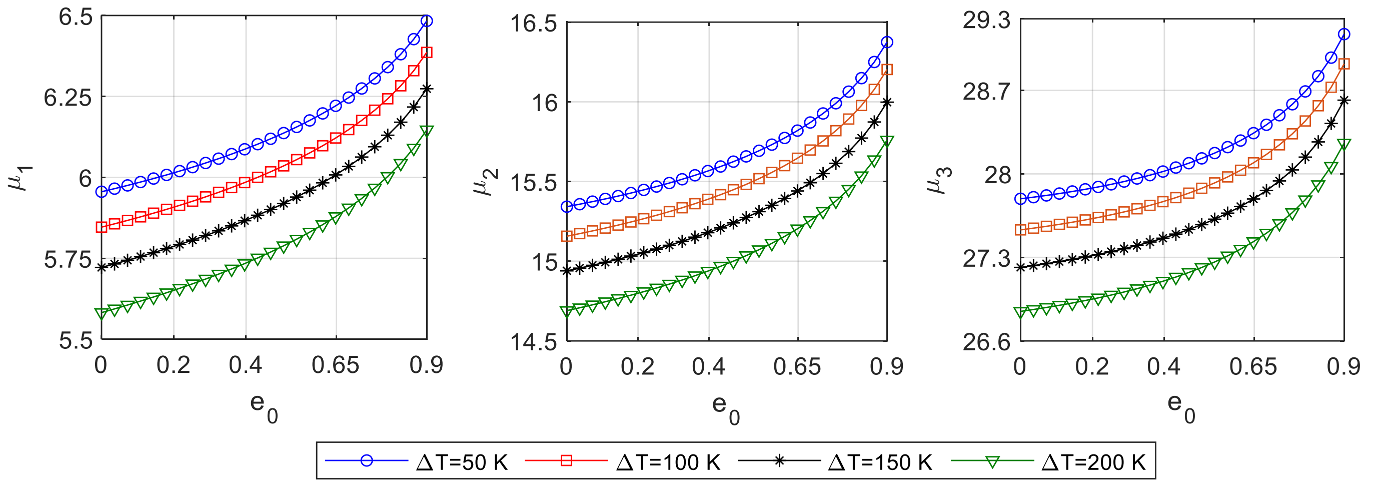

Fig. 3. The curves for the frequency parameters versus porosity coefficient of the CC (1-2-1) porous beam with porosity coefficient for L/h =10 and various values of the temperature change

Table 8. The first frequency parameters of CS beam with various sandwich configurations for different e_0 and ΔT

		L/h =5		L/h =20	
e_0	ΔT	(1-2-1)	(4-3-1)	(1-2-1)	(4-3-1)
0.2	0	3.8964	3.9108	4.4595	4.4607
	50	3.8592	3.8727	4.0358	4.0230
	100	3.8139	3.8265	3.5270	3.4952
0.4	0	3.9280	3.9464	4.5266	4.5129
	50	3.8917	3.9085	4.1222	4.0807
	100	3.8474	3.8624	3.6403	3.5611
0.6	0	3.9745	3.9802	4.6163	4.5631
	50	3.9391	3.9424	4.2304	4.1359
	100	3.8956	3.8965	3.7740	3.6239
0.8	0	4.0543	4.0122	4.7523	4.6113
	50	4.0195	3.9746	4.3826	4.1888
	100	3.9766	3.9288	3.9486	3.6839

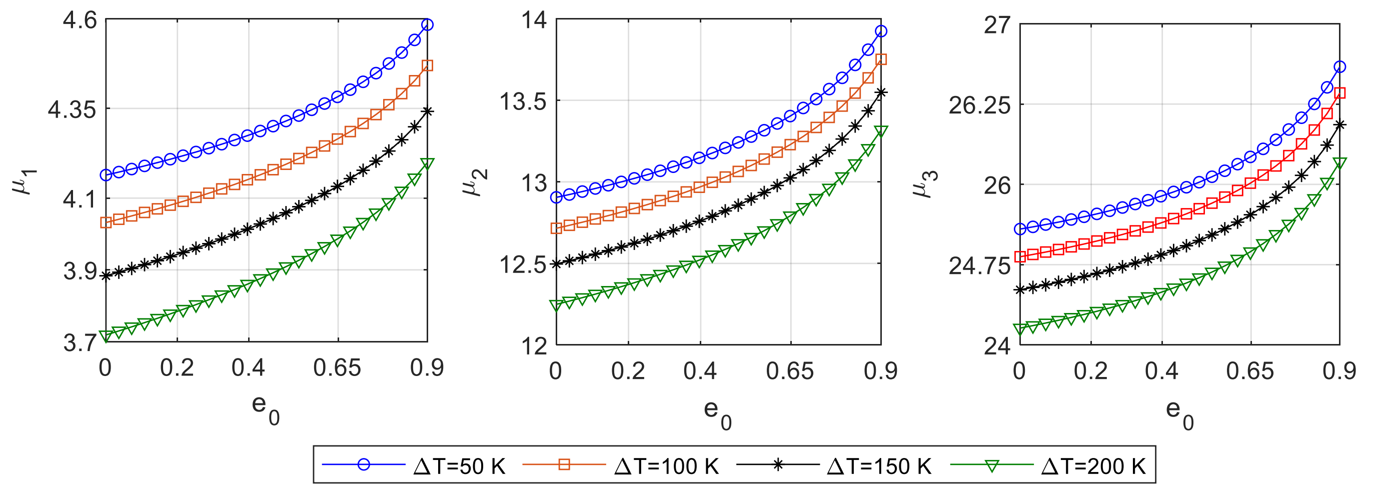

Fig. 4. The curves for the frequency parameters versus porosity coefficient of the CS (1-2-1) porous beam with porosity coefficient for L/h =10 and various values of temperature change

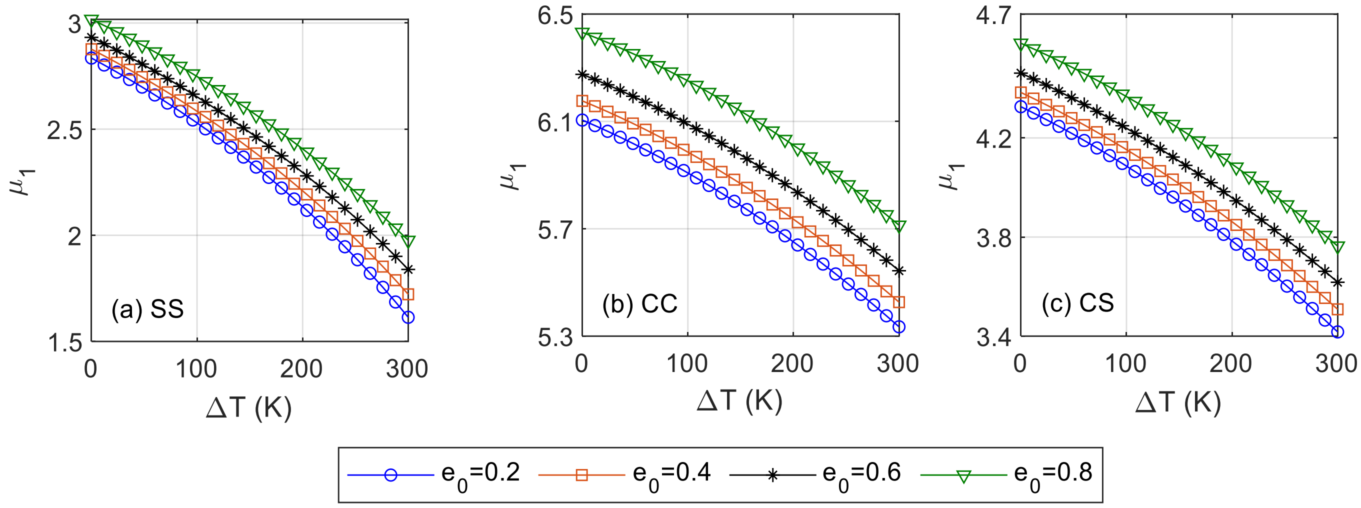

Fig. 5. The curves for the frequency parameters versus porosity coefficient of the (1-2-1) porous beam with the temperature rise for L/h =10, different porosity coefficients: (a) SS beam, (b) CC beam, (c) CS beam

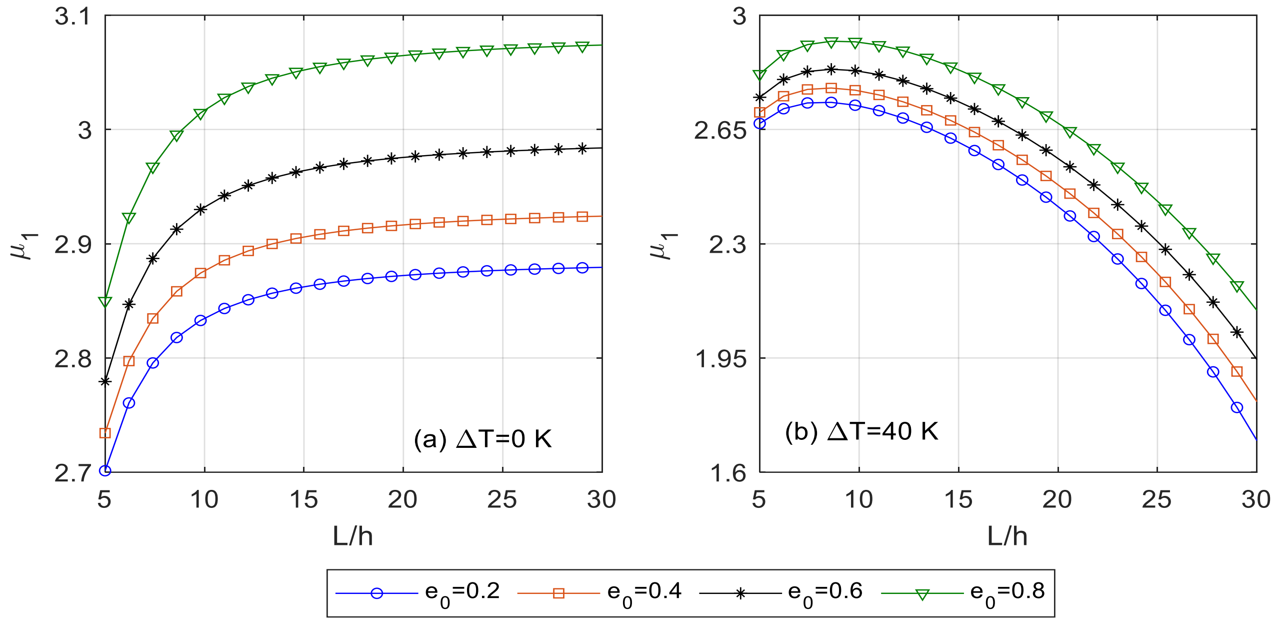

Fig. 6. Effect of aspect ratio on fundamental frequency parameter of SS (1-2-1) porous beam with different porosity coefficients: (a) ΔT=0 K, (b) ΔT=40 K

To further investigate the influence of thermal variations on the vibrational characteristics of the FGP-core sandwich beam, Fig. 5 depicts the fundamental frequency parameter as a function of temperature rise across various porosity levels. The results in the figure are presented for all three boundary conditions considered in the present work. One can see again from the figure that a significant decline in the frequency parameter occurs with the enlargement of the temperature rise, and this remark is correct for all values of the porosity coefficient and the beam end constraints. One can also observe from Fig. 5 that the impact of the porosity coefficient is the most pronounced for the beam with clamped ends, while it is the least significant for the beam with simply supported ends. Thus, the boundary conditions can alter the frequency amplitude, and they also change the vibration response to the variation of the porosity coefficient and temperature rise.

Finally, the sensitivity of the thermoelastic frequency response to the span-to-height ratio is depicted in Fig. 6 for the (1-2-1) sandwich configuration under simply supported conditions. Fig. 6 shows an interesting vibration response to the aspect ratio of the FGP sandwich beam when it is placed in a thermal environment. Without the temperature effect, the sensitivity in vibration response of the sandwich beam to the variation in the length-to-height ratio is similar to the conventional beams, and the increasing the aspect ratio enhances the fundamental frequency parameter, regardless of the porosity coefficient (see Fig. 6a). The increase in the aspect ratio lessens the effect of the shear deformation, and this is a main reason for the increase of frequency parameter. The situation has been changed when the thermal effect is effective, as shown in Fig. 6b for a temperature rise ΔT=40 K. The first frequency parameter of the sandwich beam in the thermal environment is first increased when increasing the aspect ratio, it then reaches a maximum value before decreasing, and this tendency is the same for all values of the porosity coefficient. The aspect ratio at which the frequency parameter attains the maximum value slightly increases for the sandwich beam associated with a higher porosity coefficient. Thus, the temperature not only reduces the frequencies but also changes the vibration behavior of the sandwich beam featuring an FGP core.

5. Concluding remarks

The thermomechanical vibrational behavior of FGP-core sandwich beams has been analyzed through a developed finite element model. The sandwich structure comprises two homogeneous face sheets and a functionally graded porous core, where the porosity distribution through the thickness is defined by a cosine function. The mechanical properties of the sandwich structure are considered as functions of temperature. To describe the beam's deformation and construct the governing equations, the Timoshenko beam theory was employed. The vibration analysis is then performed by establishing the discretized motion equations through the formulated finite element beam element. In order to avoid the shear-locking problem and to improve the efficient performance of the beam model, the quadratic and cubic polynomials obtained as solutions of a homogeneous equilibrium equations of a beam element are used to approximate the rotation and the transverse displacement. The frequency parameters are predicted for a sandwich beam with various boundary conditions and aspect ratios. The influence of several key parameters, including porosity distribution, porosity coefficients, thermal variations, and sandwich configurations, on the vibration of the sandwich beam are examined in detail. This study yields the following important conclusions regarding the thermomechanical response of FGP sandwich beams.

The frequency parameters increase when the porosity coefficient e_0 rises. This observed behavior holds true for all investigated boundary conditions and sandwich configurations, regardless of the magnitude of the temperature rise.

Environmental temperatures reduce the structural stiffness of the beam, consequently lowering its natural frequencies. This thermal sensitivity, however, is moderated by the presence of porosities; specifically, the impact of temperature change becomes less significant as the porosity coefficient increases.

The effect of the aspect ratio on the vibrational response is significantly influenced by temperature. As the aspect ratio increases, the frequency parameter of the sandwich beam under thermal loading initially rises to a peak value before subsequently declining.

Acknowledgments

This work was supported by Institute of Mechanics, Vietnam Academy of Science and Technology (VAST), grant number VCH.ĐTT.04/2025.

References

[1]. J. Yang, D. Chen, K. Gao (Editors). (2023). Machine Learning Aided Analysis, Design, and Additive Manufacturing of Functionally Graded Porous Composite Structures. *Woodhead Publishing. Elsevier*. DOI: 10.1016/C2022-0-00102-1

[2]. D. Chen, S. Kitipornchai, J. Yang. (2018). Dynamic response and energy absorption of functionally graded porous structures. *Materials & Design*, 140, 473-487. https://doi.org/10.1016/j.matdes.2017.12.019

[3] N. Wattanasakulpong, A. Chaikittiratana, S. Pornpeerakeat. (2018). Chebyshev collocation approach for vibration analysis of functionally graded porous beams based on third-order shear deformation theory. *Acta Mechanica Sinica*, 34, 1124-1135. https://doi.org/10.1007/s10409-018-0770-3

[4] D. Chen, J. Yang, S. Kitipornchai. (2015). Elastic buckling and static bending of shear deformable functionally graded porous beam. *Composite Structures*, 133, 54-61. https://doi.org/10.1016/j.compstruct.2015.07.052

[5] D. Chen, J. Yang, S. Kitipornchai. (2016). Free and forced vibrations of shear deformable functionally graded porous beams. International Journal of Mechanical Sciences, 108-109, 14-22. https://doi.org/10.1016/j.ijmecsci.2016.01.025

[6] B. Srikarun, W. Songsuwan, N. Wattanasakulpong. (2021). Linear and nonlinear static bending of sandwich beams with functionally graded porous core under different distributed loads. *Composite Structures*, 276, 114538. https://doi.org/10.1016/j.compstruct.2021.114538

[7] D. Chen, S. Kitipornchai, J. Yang. (2016). Nonlinear free vibration of shear deformable sandwich beam with a functionally graded porous core. *Thin-Walled Structures*, 107, 39-48. https://doi.org/10.1016/j.tws.2016.05.025

[8] Y. Chen, G. Jin, C. Zhang, T. Ye, Y. Xue. (2018). Thermal vibration of FGM beams with general boundary conditions using a higher-order shear deformation theory. *Composites Part B: Engineering*, 153, 376–386. https://doi.org/10.1016/j.compositesb.2018.08.111

[9] L.C. Trinh, T.P. Vo, H.-T. Thai, T.-K. Nguyen. (2016). An analytical method for the vibration and buckling of functionally graded beams under mechanical and thermal loads. *Composites Part B: Engineering*, 100, 152-163. https://doi.org/10.1016/j.compositesb.2016.06.067

[10] N. Wattanasakulpong, B.G. Prusty, D.W. Kelly. (2011). Thermal buckling and elastic vibration of third-order shear deformable functionally graded beams. *International Journal of Mechanical Sciences*, 53(9), 734–743. https://doi.org/10.1016/j.ijmecsci.2011.06.005

[11] D.-G. Zhang. (2014). Thermal post-buckling and nonlinear vibration analysis of FGM beams based on physical neutral surface and high order shear deformation theory. *Meccanica*, 49, 283-293. https://doi.org/10.1007/s11012-013-9793-9

[12] S. Eiadtrong, N. Wattanasakulpong, T.P. Vo. (2023). Thermal vibration of functionally graded porous beams with classical and non-classical boundary conditions using a modified Fourier method. *Acta Mechanica*, 234, 729-750. https://doi.org/10.1007/s00707-022-03401-5

[13] Y.S. Touloukian. (1967). Thermo-physical Properties of High Temperature Solid Materials. Purdue University. Thermophysical Properties Research Center. *Macmillan.*

[14] R.D. Cook, D.S. Malkus, M.E. Plesha, R.J. Witt. (2002). Concepts and Applications of Finite Element Analysis. 4th ed. *John Wiley & Sons.*

[15] J.B. Kosmatka. (1995). An improved two-node finite element for stability and natural

frequencies of axial-loaded Timoshenko beams. *Computers & Structures*, 57(1), 141–149. https://doi.org/10.1016/0045-7949(94)00595-T

[16] M. Geradin, D.J. Rixen. (1997). Mechanical Vibrations: Theory and Applications to Structural Dynamics, 2nd Edition. *John Wiley & Sons*.

[17] K. Foroutan, A. Shaterzadeh, H. Ahmadi. (2020). Nonlinear static and dynamic hygrothermal buckling analysis of imperfect functionally graded porous cylindrical shells. *Applied Mathematical Modelling*, 77, 539–553. https://doi.org/10.1016/j.apm.2019.07.062